Physical Sciences

Original article

Analytical solutions in the modeling of the endovenous laser ablation

Soluciones analíticas en la modelación de la ablación endovenosa con láser

⬤ **Luisa Consiglieri**

Independent Researcher, Lisboa, Portugal

Abstract

We modeled the operative treatment of incompetent truncal veins using endovenous laser ablation (EVLA). The main concern regarding the thermoablative technique is tissue damage, which is correlated with (1) the energy provided by the laser power and (2) temperature distribution. Our objective was to accurate the two functions, namely the fluence rate and the temperature, depending on the thermoablative technique and the endovenous laser treatment (ELT). First, we considered three differential equations: diffusion, heat, and bioheat equations in the endovenous-perivenous multidomain to describe the lumen, the vein wall, the tissue pad, and the skin. Second, we examined the power source according to the Beer-Lambert law in the incident beam irradiance and the heat source as the so-called absorbed optical power density. Third, we checked out the heat transfer at the skin boundary according to Newton's law of cooling, which stands for a Robin boundary condition. For this new model, we proposed exact solutions: applying differential equations techniques, we solved (1) a diffusion approximation of the radiative transfer equation under the considered power source, and (2) the coupled heat and bioheat equations under the considered heat source accomplished with the Robin boundary condition. Then, we graphically illustrated the fluence rate profile and discussed its time dependence and steady state. Besides, we discuss thermal damage to the vein-tissue system and present open problems.

Keywords: EVLA; fluence rate; Beer-Lambert law; Newton's law of cooling; bioheat transfer equation; exact solutions.

Resumen

Modelamos el tratamiento quirúrgico de las venas varicosas mediante ablación endovenosa con láser (E.L.A.V.). La principal preocupación en torno a la técnica termoablativa es el daño térmico, el cual se correlaciona con (1) la energía dada por la potencia del láser y (2) la distribución de la temperatura. Nuestro objetivo fue precisar las dos funciones: la tasa de fluencia y la temperatura, al usar la técnica termoablativa y el tratamiento endovenoso con láser. Primero, consideramos tres ecuaciones diferenciales, a saber, las de difusión, calor y biocalor en el sistema endovenoso-perivenoso para describir el lumen, la pared de la vena, la almohadilla de tejido y la piel. En segundo lugar, examinamos la fuente de potencia a partir de la ley de Beer-Lambert para establecer la irradiancia del haz incidente y la fuente de calor como densidad de potencia óptica absorbida. En tercer lugar, tuvimos en cuenta la transferencia de calor en el límite de la piel según la ley de enfriamiento de Newton como condición de frontera de Robin. Para este nuevo modelo propusimos soluciones exactas: la aplicación de ecuaciones diferenciales para resolver (1) la aproximación a la difusión mediante la ecuación de transferencia radiativa bajo la fuente de potencia considerada, y (2) de ecuaciones acopladas de calor y biocalor bajo la fuente de calor lograda mediante la condición de frontera de Robin. Posteriormente, se graficó la tasa de fluencia y se discutió su dependencia con respecto al tiempo y el estado estacionario. Además, se presentan aquí algunas consideraciones en torno a los daños térmicos en el sistema vena-tejido y algunos problemas aún pendientes.

Palabras clave: E.L.A.V.; tasa de fluencia; ley de Beer–Lambert; ley de enfriamiento de Newton; ecuación de transferencia de biocalor; soluciones exactas.

Introduction

Conventional high ligation and stripping (crossectomy of the saphenofemoral junction (SFJ) with great saphenous vein (GSV) stripping) and radio-frequency (RF) ablation therapies are passing their legacy to the new technologies such as the laser (and the ultrasound-guided foam sclerotherapy) in the treatment of varicose veins (**Carradice *et al*.**, 2011; **Etlik *et al*.**, 2013; **Palombi *et al*.**, 2024; **Rasmussen *et al*.**, 2011; **Theivacumar** & **Gough**, 2011). Also the extremely high degree of recurrence occurring after previous ligation and stripping of the great saphenous vein ask for the safety and efficacy of endovenous laser ablation as a posterior treatment for recurrent symptomatic saphenous insufficiency (**Anchala *et al*.**, 2010). Clinical trials have being conducted before and after the EndoVenous Laser Ablation (EVLA) treatment. Clinical studies address failure as patency or recanalization of the GSV or residual symptoms (**Firouznia *et al*.**, 2013), the occlusion, ulcer healing, paresthesia rates and postoperative pain (**Özkan** & **Saritürk**, 2012; **Rathod *et al*.**, 2010), as other adverse side effects (**Schwarz *et al*.**, 2010; **Sharif *et al*.**, 2006). In (**Tseng *et al*.**, 2022), the authors describe and report the symptom severity. Although it is unknown its cause even an ischaemic stroke following endovenous laser treatment of varicose veins is reported (**Caggiati** & **Franceschini**, 2010). In the recent years, several clinical follow-up studies (**Doganci** & **Demirkilic**, 2010; **Gale *et al*.**, 2010; **Goldman**, **Mauricio**, & **Rao**, 2004; **Min**, **Khilnani**, & **Zimmet**, 2003; **Oh *et al*.**, 2003; **Palombi *et al*.**, 2024; **Puggioni *et al*.**, 2005) have reporting different laser systems to treat incompetent GSV. Indeed, the advantages of the endovenous laser surgery are more relevant than its complications (**Ash** & **Moore**, 2010). In (**Palombi *et al*.**, 2024), the efficacy and safety endpoints after the EVLA treatment are carried out.

The fibre type is the single most significant factor related to treatment outcome (**Prince *et al*.**, 2011). For effective endovenous laser (EVL) therapy, the laser wavelength varies from $\lambda = 810\,\text{nm}$ (**Sharif *et al*.**, 2006; **Theivacumar** & **Gough**, 2011) until to 980 nm (**Schmedt *et al*.**, 2010), at power settings of 9 W to 17 W (**Rathod *et al*.**, 2010) according to the diameter and severity of varicose veins. The 1470-nm wavelength EVL system successfully closes saphenous veins but not acts as "anesthesia-less thermal ablation technology" (**Almeida *et al*.**, 2009). In (**Proebstle *et al*.**, 2004), the authors found that after EVLA with low-energy density, worse results and more relapses could be expected than with higher-energy doses.

A vast literature has been playing a prominent and broad-spectrum role in the study of the temperature dependence of the thermophysical and mechanical properties of biological tissues (see (**Bianchi *et al*.**, 2022) and the references therein). The aim of some studies is to determine how the heat sink effect of the blood flow inside the vessel may either be measured (**Consiglieri**, 2012; **Consiglieri**, dos **Santos**, & **Haemmerich**, 2003; **Kotte**, van **Leeuwen**, & **Lagendijk**, 1999), distort coagulation volume during thermal therapies (**Horng *et al*.**, 2007; **Vuylsteke *et al*.**, 2011), or protect the vessel wall in the proximity of an RF-assisted resection device (**González-Suárez *et al*.**, 2014). In this last work, the tissue vaporization was modelled by the enthalpy method, while parametric studies were conducted in (**Consiglieri**, 2012) to prove the blood flow has a cooling effect during RF ablation treatment. The present goal goes somewhat on the opposite direction: to study how the laser wavelength behaves and the damage of blood vessels is influenced.

The finding of mathematical models is essential to control the temperature, and to prevent postoperative complications. It includes handling of mathematical problems generated by the application of models to real thermal conditions. The combination Mordon's optical-thermal model with the presence of a strongly absorbing carbonized blood layer on the fibre tip is introduced in (**Van Ruijven *et al*.**, 2014) by neglecting the Arrhenius damage integral, and after is developed in (**Poluektova *et al*.**, 2014). We refer to (**Marqa *et al*.**, 2013) a finite element modelling of the influence of air cooling that simulates the perisaphenous subcutaneous tumescent saline solution infiltration. In (**Katta *et al*.**, 2022) a finite element

model is developed for the study of the limitation in laser coagulation of large diameter blood vessels during irradiation. Global unique solvability of the conductive heat transfer problem is proved in (**Chebotarev**, **Pak**, & **Kovtanyuk**, 2023) and numerical analysis is presented to evaluate the behaviour of temperature fields. Some analytical solutions to the bioheat transfer problem are studied in multiregion (**Consiglieri**, 2016; **Consiglieri**, 2013), where the Joule effect is assumed to be constant.

Here, we follow the whole path from the phenomenological interpretation of thermal therapy to scientific computing for producing simulations. Our objective is to accurate the heat source by establishing explicit expressions for (1) the fluence rate and (2) the temperature, whose expressions can be implemented in computer programs. Bearing this in mind, we firstly state a new mathematical model. Then, this new model is analytically solved such that the final results will be very fast to execute. To validate our model, we compare our results with experimental measurements.

The structure of the present work is as follows. Next section, we state the model under study, in the endovenous-perivenous multidomain, describing the lumen, the vein wall, the tissue pad and the skin. In first subsection, we consider a diffusion approximation of the radiative transfer equation taking the Beer–Lambert law into account in the irradiance of the incident beam. In second subsection, we consider the heat and the bioheat equations, under the heat source as dependent on the first subsection. Moreover, we consider the heat transfer at the skin boundary according to the Newton law of cooling. Last subsection addresses the dimensionless indicator of damage. Section auxiliary solutions covers the methodology for the derivation of the exact solutions in cylindrical coordinates. We use the method of separation of variables, in particular, the Bernoulli–Fourier technique in first subsection. Second subsection covers a particular solution according to Duhamel principle. We present the results and discussions and make some concluding remarks in the last two sections, respectively.

Mathematical model

The optical laser fibre is inserted into the sheath so that the fibre tip extends $2\,\mathrm{cm}$ beyond the end of the sheath to avoid the melting of the sheath material (**Schmedt** *et al*., 2010; **Sharif** *et al*., 2006). The geometry of the fibre–tissue system is assumed to be as follows (cf. Fig. 1). The fibre probe (with radius r_f) is assumed to be centred in the middle of the vein, where the vein segment $\Omega_\mathrm{v} = \Omega_\mathrm{lumen} \cup \Omega_\mathrm{w}$ is assumed to be cylindrical with r_i and ε being the inner radius and the thickness of the venous wall, respectively. In vivo, the thickness of the venous wall is approximately one tenth the width of its blood column: $\varepsilon = r_\mathrm{i}/5$.

The saphenous vein is considered to be parallel to the skin surface (**Marqa** *et al*., 2013). Then, the complete domain $\Omega = \Omega_\mathrm{v} \cup \Omega_\mathrm{pad} \cup \Omega_\mathrm{skin}$ is assumed to be constituted by axially half-cylindrical volumes, namely vein, perivenous and skin tissues. The tissue around the venous may be considered homogenous. The thickness of the perivenous and skin tissues are $l_\mathrm{pad} = 10\,\mathrm{mm}$ and $l_\mathrm{skin} = 3\,\mathrm{mm}$, respectively.

The procedure begins by inserting the laser sheath and positioning the bare tip below SFJ. At time $t = 0$, the fibre tip is located at axial coordinate z_0. The fibre is kept in a piecewise pull-back model until the level of the knee, with each pulling back of the fibre being at a constant velocity v. During the off period, the laser fibre and the introduced catheter are pulled back by increments, and then a further irradiation pulse is activated. This cycle is repeated until a desired fixed distance. The piecewise pull-back in the application of laser light is preferred because the manually made continuous pull-back depends on the operating surgeon technique and experience. For each fixed irradiation time $t_\mathrm{end} > 0$, $L > 0$ stands for the corresponding length of the treated vein segment.
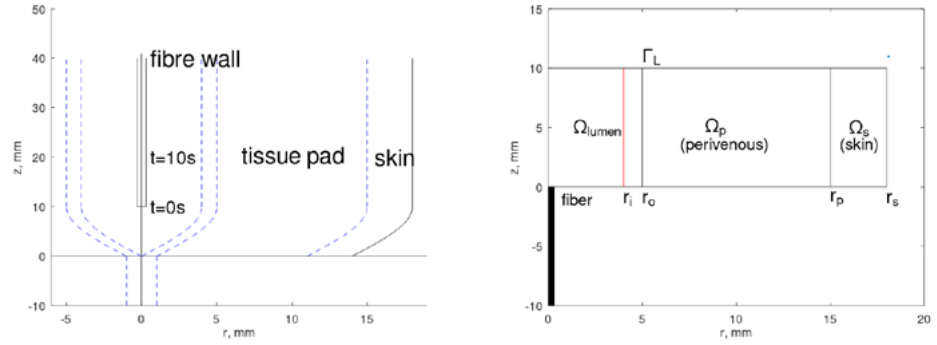
Figure 1. (a) Schematic sagittal representation of the endovenous fibre at the initial instant of time $t = 0$. (b) Schematic cylindrical representations in 2D of the lumen $\Omega_{\text{lumen}} = \{(x,y) \in \mathbb{R}^2 : x^2 + y^2 < r_i^2\} \times]0; L[$, the wall $\Omega_w = \{(x,y) \in \mathbb{R}^2 : r_i^2 < x^2 + y^2 < (r_i + \varepsilon)^2\} \times]0; L[$, the tissue pad $\Omega_{\text{pad}} = \{(x,y) \in \mathbb{R}^2 : (r_i + \varepsilon)^2 < x^2 + y^2 < r_p^2\} \times]0; L[$, and the skin $\Omega_{\text{skin}} = \{(x,y) \in \mathbb{R}^2 : r_p^2 < x^2 + y^2 < r_s^2\} \times]0; L[$.

We assume that outer surface $\Gamma_L = \{(x,y) : x^2 + y^2 < r_s^2\} \times \{L\}$ is an insulating boundary, that is, there is no outflow.

Diffusion approximation of the radiative transfer equation

The light power emitted out of the fibre tip into the ambient blood is scattered towards the vein wall and the surrounding tissue. The fluence rate ϕ [W m^{-2}] verifies the diffusion equation (**Star**, 1995)

$$\frac{1}{v}\frac{\partial \phi}{\partial t} - D\Delta\phi + \mu_a\phi = S \qquad \text{in } \Omega \times]0; t_{\text{end}}[, \tag{1}$$

where:

$v = c/n$ is the speed of light in the tissue [m s^{-1}], as determined by the relative refractive index n;

$D = \frac{1}{3(\mu_a + \mu_s')}$ is the diffusion coefficient;

μ_a is the absorption coefficient [m^{-1}];

$\mu_s' = (1 - g)\mu_s$ is the reduced scattering coefficient [m^{-1}], with g being the scattering anisotropy coefficient, and μ_s being the scattering coefficient;

S is the source of scattered photons [W m^{-3}], which represents the power injected in the unit volume.

Usually S is assumed to be a source point in order to use the Green functions in the determination of the solution ϕ of the diffusion equation (1). For a single spherically symmetric point source emitting P_{laser} [W], the form of ϕ at a distance r from the source is $P_{\text{laser}}\exp(-\mu_{\text{eff}}r)/(4\pi Dr)$ (**Mordon**, **Wassmer**, & **Zemmouri**, 2006), where $\mu_{\text{eff}} = \sqrt{3\mu_a(\mu_a + \mu_s')}$ represents the effective attenuation coefficient.

Laser energy is delivered along the vein with a continuous emission (**Anchala *et al.***, 2010), and a fibre pull-back is kept at about 1-cm increment every 10 seconds (**Ash & Moore**,

2010). In this work, we consider

$$S(r,z,t) \equiv S(r_\mathrm{f},z,t) = \frac{P_\mathrm{laser}}{\pi r_\mathrm{f}^2} \frac{\mu_\mathrm{s}(\mu_\mathrm{t}+g\mu_\mathrm{a})}{\mu_\mathrm{a}+\mu_\mathrm{s}'} \exp[-\mu_\mathrm{t}(z+vt)], \tag{2}$$

for all $(r,z,t) \in [0;r_\mathrm{f}[\times]-vt;L[\times[0;t_\mathrm{end}[$. Here, $\mu_\mathrm{t} = \mu_\mathrm{a} + \mu_\mathrm{s}$ stands for the attenuation coefficient *i.e.* the reciprocal of the average distance light travels before being scattered or absorbed by the medium. The above expression stands for the Beer–Lambert law (**Prahl**, 1995) when $t = 0$, while stands for the velocity of the fibre pull-back with increment $L = 10\,\mathrm{mm}$ and time $t_\mathrm{end} = 10\,\mathrm{s}$, *i.e.* at a velocity $v = 1.0\,\mathrm{mm\,s}^{-1}$.

Heat transfer

The heat energy was delivered directly to the vein wall (**Sharif *et al*.**, 2006), due to that the compression reduces the vein diameter. The heat transfer due to the energy of light deposited is described by the following heat and bioheat transfer equations:

in $\Omega_\mathrm{lumen}\times]0;t_\mathrm{end}[$:

$$\rho c_\mathrm{p}\left(\frac{\partial T}{\partial t}+\mathbf{u}\cdot\nabla T\right) = \nabla\cdot(k\nabla T)+q \tag{3}$$

in $\left(\Omega_\mathrm{w}\cup\Omega_\mathrm{p}\cup\Omega_\mathrm{s}\right)\times]0;t_\mathrm{end}[$:

$$\rho c_\mathrm{p}\frac{\partial T}{\partial t}+c_\mathrm{b}\omega(T-T_\mathrm{b}) = \nabla\cdot(k\nabla T)+q \tag{4}$$

where:

T is the temperature [K];

$\mathbf{u}$ is the blood velocity vector [$\mathrm{m\,s}^{-1}$];

ρ is the density [$\mathrm{kg\,m}^{-3}$];

c_p is the specific heat capacity per unit mass [$\mathrm{J\,kg}^{-1}\,\mathrm{K}^{-1}$];

k is the thermal conductivity [$\mathrm{W\,m}^{-1}\,\mathrm{K}^{-1}$];

q is the heat source caused by laser power [$\mathrm{W\,m}^{-3}$].

Considering laminar flow, the blood velocity is scalar, and the convective term in (3) reads $u\frac{\partial T}{\partial z}$. In the heat equation (3), $\rho = \rho_\mathrm{b}$ and $c_p = c_\mathrm{b}$ denote the density and the specific heat capacity of the blood, respectively. The Pennes bioheat transfer equation (4), which distinguishes itself from nonliving systems, includes the effects of blood perfusion $\omega = \rho_\mathrm{b}w$ [$\mathrm{kg\,m}^{-3}\,\mathrm{s}^{-1}$] that occurs in the capillary bed, that is, the energy transfer term $-c_\mathrm{b}\omega(T-T_\mathrm{b})$ is consequence of the mass transport of blood through tissue (cf. Table 1). Here, T_b represents the temperature of the blood (assumed to be $38\,^\circ\mathrm{C}$), w denotes the volumetric flow [s^{-1}], and $c_\mathrm{b}\omega$ accounts for the heat conducted in direction of the contribution of flowing blood to the overall energy balance, before the critical coagulation temperature.

Table 1. Thermal parameters (**Marqa** *et al*., 2013; **Mordon**, **Wassmer**, & **Zemmouri**, 2006).

	unit	blood	vein wall	perivenous tissue	skin
k	$\mathrm{W\,m^{-1}\,{}^\circ C^{-1}}$	0.52	0.53	0.21	0.21
ρ	$\mathrm{kg\,m^{-3}}$	1060	1080	1000	1109
c_p	$\mathrm{J\,kg^{-1}\,{}^\circ C^{-1}}$	3600	3690	2350	3500
ω	$\mathrm{kg\,m^{-3}\,s^{-1}}$		1.08	1	0.5545
A	$\mathrm{s^{-1}}$	7.6e+66	5.6e+63	5.6e+63	3.1e+98
E_a	$\mathrm{J\,mol^{-1}}$	4.48e+05	4.30e+05	4.30e+05	6.28e+05

The heat source q is induced by the conversion of laser light into heat, the so-called absorbed optical power density, since the heat generated by body metabolism is negligible. The distribution of absorbed energy within the irradiated volume is governed both by the absorption and the scattering properties of the tissue at the specific wavelength used:

$$q = \mu_\mathrm{a}\phi. \tag{5}$$

The heat exchange on the skin surface is given by the Newton law of cooling

$$k\frac{\partial T}{\partial r} + h_\mathrm{air}(T - T_\mathrm{air}) = 0 \tag{6}$$

if $r = r_\mathrm{s}$, $-vt < z < L$ and $t > 0$. Here, h_air is the heat transfer coefficient of the air, and T_air denotes the room temperature. In (**Marqa** *et al*., 2013), h_air is assumed to obey an equation that involves the thermal conductivity of the air, the characteristic length of flow domain, and the Prandtl and Reynolds numbers.

On the remaining boundary, no heat transfer outflow is assumed:

$$\frac{\partial T}{\partial z}(r,z,t) = 0 \qquad \text{if } 0 < r < r_\mathrm{s},\ z = -vt, L, \text{ and } t > 0.$$

Thermal damage to the vein-tissue system

Thermal damage is consequence of the water content of the constituent cells reaches $100\,^\circ\mathrm{C}$. By this reason, the main predictor of the thermal damage is the dense microbubble formation that is commonly seen at the area.

Let t_crit be the time correspondent to the dimensionless indicator of damage when it is equal to one: $\Omega(t_\mathrm{crit}) = 1$, *i.e.* from the Arrhenius burn integration

$$\frac{1}{A} = \int_0^{t_\mathrm{crit}} \exp\left[-\frac{E_\mathrm{a}}{RT(r,z,\tau)}\right]\mathrm{d}\tau, \tag{7}$$

where R is the universal gas constant ($8.314\,\mathrm{J\,mol^{-1}\,K^{-1}}$), A is a frequency factor $[\mathrm{s^{-1}}]$, and E_a is the activation energy for the irreversible damage reaction $[\mathrm{J\,mol^{-1}}]$. Approximating the above integral by the lower and upper Riemann sums with the partition constituted by a finite number M of subintervals of $]0, t_\mathrm{crit}[$, of equal length, t_crit obeys

$$\sum_{m=1}^{M} \exp\left[-\frac{E_\mathrm{a}}{RT\left(r,z,\frac{m}{M}t_\mathrm{crit}\right)}\right] < \frac{M}{At_\mathrm{crit}} < \sum_{m=1}^{M} \exp\left[-\frac{E_\mathrm{a}}{RT\left(r,z,\frac{m-1}{M}t_\mathrm{crit}\right)}\right]. \tag{8}$$

Auxiliary solutions

There exist several processes of derivation of the required solutions (**Özisik**, 2012). Here, we firstly use the method of separation of variables to find a family of elementary solutions to the parabolic equation and the boundary condition, and then the principle of superposition to construct a solution satisfying the initial condition. Hereafter, the domain subscripts are dropped out by the sake of simplicity whenever the meaning of the parameters is well understood in each domain.

In cylindrical coordinates, the Laplace operator reads (see, for instance, (**Özisik**, 2012, p. 9))

$$\Delta = \frac{\partial^2}{\partial r^2} + \frac{1}{r}\frac{\partial}{\partial r} + \frac{1}{r^2}\frac{\partial^2}{\partial \theta^2} + \frac{\partial^2}{\partial z^2},$$

with $(r, \theta, z, t) \in]0; r_o[\times] - \pi; \pi[\times]0; L[\times]0; t_{end}[$, where $r = \sqrt{x^2 + y^2}$ and θ is the polar angle measured down from the vertical axis z.

Taking the angular symmetry, we seek for solutions of the generic PDE:

$$\alpha\frac{\partial v}{\partial t} + b\frac{\partial v}{\partial z} - a\left(\frac{\partial^2 v}{\partial r^2} + \frac{1}{r}\frac{\partial v}{\partial r} + \frac{\partial^2 v}{\partial z^2}\right) + Bv = f, \tag{9}$$

defined in $]0; r_o[\times]0; L[\times]0; t_{end}[$, with v_0 denoting the initial datum, $a > 0$, and $\alpha, b, B \geq 0$.

For our purposes, we begin by exemplifying the decomposition followed for the particular function

$$f(r, z, t) = f(t)\chi_{[0;r_f]}(r)\exp[\iota z],$$

where $\iota \in \mathbb{R}$ and $\chi_{[0;r_f]}$ stands for the characteristic function over the interval $[0; r_f]$.

Thanks to the Duhamel principle, we look for a solution which can be of the form

$$v(r, z, t) = \chi_{[0;r_f]}(r)\left(\int_0^t f(s)v_3(r, z, t-s)\mathrm{d}s\right)\exp[\iota z] + C + v_1(r, z, t), \tag{10}$$

for some constant C whenever $f \equiv BC$, and v_1 solves (as described in next subsection)

$$\alpha\frac{\partial v_1}{\partial t} = a\left(\frac{1}{r}\frac{\partial}{\partial r}\left(r\frac{\partial v_1}{\partial r}\right) + \frac{\partial^2 v_1}{\partial z^2}\right) - b\frac{\partial v_1}{\partial z} - Bv_1; \tag{11}$$

$$\frac{\partial v_1}{\partial t}(r, -L, t) = \frac{\partial v_1}{\partial z}(r, L, t) = 0, \quad \forall r, t; \tag{12}$$

$$v_1(r, z, 0) = v_0(r, z), \quad \forall r, z, \tag{13}$$

and v_3 solves

$$\alpha\frac{\partial v_3}{\partial t} + b\frac{\partial v_3}{\partial z} + (B + b\iota - a\iota^2)v_3 = a\left(\frac{1}{r}\frac{\partial}{\partial r}\left(r\frac{\partial v_3}{\partial r}\right) + \frac{\partial^2 v_3}{\partial z^2}\right); \tag{14}$$

$$v_3(r, z, 0) = 1/\alpha, \quad \forall r, z, \tag{15}$$

such that

$$-a\frac{\partial v}{\partial r}(r_s, z, t) + hv(r_s, z, t) = h\gamma, \quad \forall z, t, \tag{16}$$

for some $\gamma \geq 0$.

We may consider $v_3(t) = \exp[\zeta t]/\alpha$ with $\zeta = (a\iota^2 - b\iota - B)/\alpha$.

Analytical solutions

Using Bernoulli–Fourier technique, the Cauchy–Robin–Neumann problem admits a solution of the form:

$$v_1(r,z,t) = R(r)Z(z)F(t).$$

In order to obtain an analytical solution, let us take the system of ordinary differential equations (ODE)

$$\begin{cases} F'(t) = \zeta F(t) \\ Z''(z) - (b/a)Z'(z) = \eta^2 Z(z) \\ (rR'(r))' = \beta r R(r), \end{cases} \tag{17}$$

with $\alpha\zeta = a(\beta + \eta^2) - B$. The solution of the first ODE is $F(t) = A_0 \exp[\zeta t]$, for some constant A_0.

The elementary solutions for Z are

$$\exp\left[\left(\frac{b}{2a} \pm \Xi\right)z\right],$$

where $\Xi = (2a)^{-1} \sqrt{b^2 + 4a^2\eta^2}$.

The elementary solutions for R are the Bessel functions of first and second kind and order 0, respectively, $J_0(\sqrt{|\beta|}r)$ and $Y_0(\sqrt{|\beta|}r)$ if $\beta < 0$; or the modified Bessel functions of first and second kind and order 0, respectively, $I_0(\sqrt{\beta}r)$ and $K_0(\sqrt{\beta}r)$ if $\beta > 0$ (**Özisik**, 2012).

We recall their Taylor series expansions around the origin

$$J_0(r) = \sum_{n=0}^{\infty} \frac{(-1)^n}{2^{2n}} \frac{r^{2n}}{n!\Gamma(n+1)};$$

$$Y_0(r) = \frac{2}{\pi}\left(J_0(r)\ln\left[\frac{r}{2}\right] - \sum_{n=0}^{\infty}(-1)^n \frac{1 + (1/2) + \cdots + (1/n) - \gamma}{2^{2n}(n!)^2}r^{2n}\right);$$

$$I_0(r) = \sum_{n=0}^{\infty} \frac{1}{2^{2n}} \frac{r^{2n}}{n!\Gamma(n+1)};$$

$$K_0(r) = -I_0(r)\ln\left[\frac{r}{2}\right] + \sum_{n=0}^{\infty} \frac{1 + (1/2) + \cdots + (1/n) - \gamma}{2^{2n}(n!)^2}r^{2n},$$

where Γ is the gamma function and γ is the Euler–Mascheroni constant. Moreover, the following wronskian relationships

$$J_1(\beta r)Y_0(\beta r) - Y_1(\beta r)J_0(\beta r) = \frac{2}{\pi\beta r}; \tag{18}$$

$$K_1(\beta r)I_0(\beta r) + I_1(\beta r)K_0(\beta r) = \frac{1}{\beta r} \tag{19}$$

hold, for any $\beta > 0$ (see (**Özisik**, 2012, p. 672) and (**Olver**, 1972, pages 360 and 375)).

Considering $\upsilon_0 = 0$ in Ω_{lumen} and taking $\beta = -\beta_{1,j}^2$ according to $j =$ wall, pad or skin, we find

$$v_1(r,z,t) = \begin{cases} 0 & \text{in } \Omega_{\text{lumen}} \\ A(r)Z(z)\exp[\zeta t] & \text{otherwise,} \end{cases} \tag{20}$$

where

$$A(r) := \begin{cases} A_{1,w}(Y_0(\beta_{1,w}r_{\text{i}})J_0(\beta_{1,w}r) - J_0(\beta_{1,w}r_{\text{i}})Y_0(\beta_{1,w}r)) & \text{in } \Omega_{\text{w}} \\ A_{1,p}J_0(\beta_{1,p}r) + A_{2,p}Y_0(\beta_{1,p}r) & \text{in } \Omega_{\text{p}} \\ A_{1,s}J_0(\beta_{1,s}r) + A_{2,s}Y_0(\beta_{1,s}r) & \text{in } \Omega_{\text{s}} \end{cases}$$

and the Neumann condition (12) implies that

$$Z(z) = \exp\left[\frac{b}{2a}z\right]\left(b\sinh\left[\Xi(L-z)\right] + \sqrt{b^2 + 4a^2\eta^2}\cosh\left[\Xi(L-z)\right]\right). \qquad (21)$$

The above involved constants may be determined by using the continuity conditions on the fluxes and on the functions themselves.

In particular, by the homogeneous Robin condition (16), we have

$$a\beta_{1,s}\left(A_{1,s}J_1(\beta_{1,s}r_s) + A_{2,s}Y_1(\beta_{1,s}r_s)\right) + h\left(A_{1,s}J_0(\beta_{1,s}r_s) + A_{2,s}Y_0(\beta_{1,s}r_s)\right) = 0.$$

Notice that if $\gamma > 0$ then we have an additional relation, which can be analysed by adding an additional solution of the form $R(r) = A_1I_0(\sqrt{B/a}r) + A_2K_0(\sqrt{B/a}r)$ that obeys

$$-\sqrt{aB}\left(A_1I_1(\sqrt{\frac{B}{a}}r_s) - A_2K_1(\sqrt{\frac{B}{a}}r_s)\right) + hR(r_s) = h\gamma.$$

Particular solution

In this section, we rephrase the particular solution, according to Duhamel principle, in (10)

$$\left(\int_0^t f(s)v_4(r,z,t-s)\mathrm{d}s\right)R(r)\exp[\iota z]$$

by taking $f(r,z,t) = f(t)R(r)\exp[\iota z]$, where $\iota \in \mathbb{R}$ and R denotes any of the Bessel functions of order 0, namely, $J_0(\sqrt{|\beta|}r)$ and $Y_0(\sqrt{|\beta|}r)$ if $\beta < 0$; or the modified Bessel functions of order 0, namely, $I_0(\sqrt{\beta}r)$ and $K_0(\sqrt{\beta}r)$ if $\beta > 0$, introduced in above subsection. Analogously, we may consider a solution $v_4(t) = \exp[\zeta t]/\alpha$ with $\zeta = \left(a(\iota^2 + \beta) - b\iota - B\right)/\alpha$.

Results and discussions

The fluence rate ϕ, defined in blood whenever the source $S \neq 0$ (cf. (2)), can be assumed independent on the radius r as satisfying (9) with $\alpha = 1/v$, $b = 0$, $a = D$, $B = \mu_a$ and $f = S$, with $\iota = -\mu_t$. Thus, we may choice the particular functions $v_2 = 0$ and $v_3(t) = v\exp[\zeta t]$, with

$$\zeta := v(D\mu_t^2 - \mu_a) > 0$$

according to Table 2.

Table 2. Optical parameters (**Marqa** *et al*., 2013; **Van Ruijven** *et al*., 2014) (at slow shear rate (**Roggan** *et al*., 1999)).

λ [nm]	μ_a [mm^{-1}]				μ_s' [mm^{-1}]			
	blood	vein wall	tissue pad	skin	blood	vein wall	tissue pad	skin
810	0.21	0.2	0.017	0.2	0.73	2.4	1.2	0.9
980	0.21	0.1	0.03	0.10	0.6	2.0	1.0	0.81
1064	0.12	0.12	0.034	0.10	0.58	1.95	0.98	0.77

Then, we have

$$\phi_v(r,z,t) = \frac{vS(r_f,z,0)}{\zeta + \mu_t v}\exp[\zeta t]\left(1 - \exp[-(\zeta + \mu_t v)t]\right),$$

for $0 \leq r < r_f$, $-L < z < L$ and $0 \leq t < t_{end}$. Typically, a laser fibre for medical applications has a 600-micron diameter ($r_f = 0.3\,mm$).

Next, by the interface continuity conditions, ϕ_v can be extended as a solution at the position (r, z) and the time t. If $r_f < r \leq r_i$ ($j = $ blood)

$$\phi_v(r,z,t) = \frac{vS(r_f,z,0)}{\zeta + \mu_t v} \exp[\zeta t] + \Big(B_1 J_0(\beta_j r) + B_2 Y_0(\beta_j r)\Big) \exp[-\mu_t(z + vt)];$$

and otherwise

$$\phi_v(r,z,t) = (B_3 I_0(\varkappa_j r) + B_4 K_0(\varkappa_j r)) \exp[-\mu_t z + \zeta t]$$
$$+ (B_5 J_0(\beta_j r) + B_6 Y_0(\beta_j r)) \exp[-\mu_t(z + vt)],$$

where the abstract constants $B_1, \cdots, B_6$ are defined by the boundary and interface continuity conditions. The parameters, $\varkappa_j$ and β_j, are determined due to that the PDE (1) is verified by the function ϕ, namely

$$\zeta/v_j + \mu_a^{(j)} = D_j\left(\mu_t^2 + \varkappa_j^2\right) \quad j = \text{wall}, \text{pad}, \text{skin};$$
$$-\frac{\mu_t v}{v_j} + \mu_a^{(j)} = D_j\left(\mu_t^2 - \beta_j^2\right) \quad j = \text{blood}, \text{wall}, \text{pad}, \text{skin}.$$

That is,

$$\varkappa_j = \sqrt{\frac{n_{tissue}}{n_{blood}} \frac{D\mu_t^2 - \mu_a}{D_j} + (\mu_{eff}^{(j)})^2 - \mu_t^2} > 0;$$

$$\beta_j = \sqrt{\mu_t^2 - (\mu_{eff}^{(j)})^2 + \frac{\mu_t v}{v_j D_j}} > 0.$$

Here, we may consider $n = 1.4$ for both the blood and the tissues.

This solution proves that the problem is ill-posed. Although it gives a good answer at the scale of picoseconds ($c = 0.3\,mm\,ps^{-1}$), it is inadequate for describing the behaviour of the fluence rate whenever the fibre moves. The unsteady ϕ should solves (1) at the steady state, being such that ϕ attains its maximum at $z = -vt$. Then, we have

if $0 \leq r < r_f$:

$$\phi(r,z,t) = B_0 \exp[-\mu_{eff}(z + vt)] - \frac{S(r_f, 0, 0)}{D\mu_t^2 - \mu_a} \exp[-\mu_t(z + vt)]; \tag{22}$$

if $r_f < r \leq r_i$:

$$\phi(r,z,t) = B_0 \exp[-\mu_{eff}(z + vt)] + \Big(B_1 J_0(\beta_b r) + B_2 Y_0(\beta_b r)\Big) \exp[-\mu_t(z + vt)]; \tag{23}$$

otherwise:

$$\phi(r,z,t) = (B_3 W_3(\varkappa_{\lambda,j} r) + B_4 W_4(\varkappa_{\lambda,j} r)) \exp[-\mu_{eff}(z + vt)]$$
$$+ (B_5 J_0(\beta_j r) + B_6 Y_0(\beta_j r)) \exp[-\mu_t(z + vt)], \tag{24}$$

where the abstract constants $B_0, B_1, \cdots, B_6$ are defined by the initial, boundary and interface continuity conditions. We consider the modified Bessel functions $W_3 = I_0$ and $W_4 = K_0$ if $\lambda = 810; 1064$ and $j = $ wall, skin, or $\lambda = 980$ and $j = $ wall; and the Bessel functions $W_3 = J_0$ and $W_4 = Y_0$ otherwise, in accordance to the factors of the $r-$argument
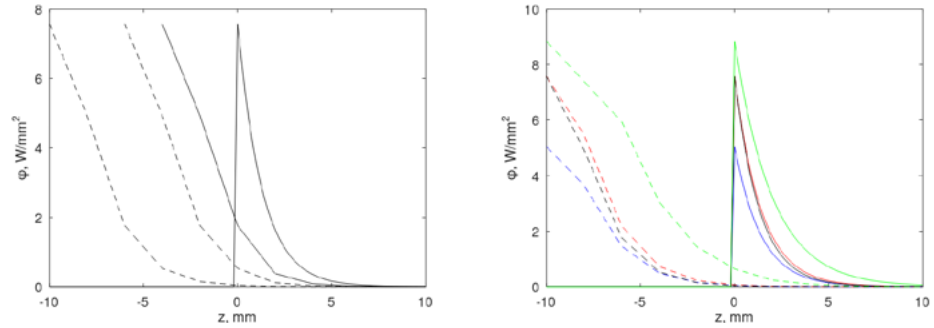
Figure 2. (a) Graphical representations of ϕ, at the wavelength of 810 nm, for different instants of time. (b) Graphical representations of ϕ for the wattage set at 15 W: with wavelengths of 810 nm (in black) and 980 nm (in red) and at 10 W: with wavelengths of 980 nm (in blue) and 1064 nm (in green). Solid lines stand for the initial instant of time, while dashed lines stand for the final instant of time.

if $\lambda = 810; 1064$:

$$\varkappa_{\lambda,j} = \begin{cases} \sqrt{(\mu_{\text{eff}}^{(j)})^2 - \mu_{\text{eff}}^2} > 0 & j = \text{wall}, \text{skin}; \\ \sqrt{\mu_{\text{eff}}^2 - (\mu_{\text{eff}}^{(j)})^2} > 0 & j = \text{pad}, \end{cases} \tag{25}$$

if $\lambda = 980$:

$$\varkappa_{\lambda,j} = \begin{cases} \sqrt{(\mu_{\text{eff}}^{(j)})^2 - \mu_{\text{eff}}^2} > 0 & j = \text{wall}; \\ \sqrt{\mu_{\text{eff}}^2 - (\mu_{\text{eff}}^{(j)})^2} > 0 & j = \text{pad}, \text{skin}, \end{cases} \tag{26}$$

and for $j = $ blood, wall, pad, skin:

$$\beta_j = \sqrt{\mu_t^2 - (\mu_{\text{eff}}^{(j)})^2} > 0. \tag{27}$$

Parameters, used in clinical procedures, are known: the power is set at 15 W (with wavelengths of 810 nm and 980 nm) and at 10 W (with wavelengths of 980 nm and 1064 nm). Calculations use Octave software, under the optical parameters in Table 2. Figure 2 (a) shows the ϕ-profile to the power of 15 W and the wavelength of 810 nm at different instants of time, considering the continuous movement of the fibre tip. The slope decreases from the initial instant of time (solid line) $z = t = 0$ until the final instant of time (dashed line) $z = -10, t = 10$, which reflects the accumulation of the fluence rate. Figure 2 also illustrates the higher distributions only under the tip, as it is experimentally consistent.

As expected, Figure 2 (b) shows similar profiles between different wavelengths and set powers. At the wavelength of 980 nm, the 15 W-curves (in red) has higher values than the 10 W-curves (in blue). At the power 15 W, the 810 nm-curves (in black) and the 980 nm-curves (in red) match each other, while at the power 10 W, the slope of 980 nm-curves (in blue) is similar than the slope of 1064 nm-curves (in green), but there is no match.

This evaluation improves the study of the absorbed volumetric power q, and consequently it will improve the study of the distribution of the temperature and make the simulation of the heat transfer closer to reality. Our results are consistent to that the use of laser energies of various wavelengths has no significant difference in their effectiveness and complication rate (**Memetoglu**, **Erbasan**, & **Özel**, 2012).

Hereafter, we assume the solution ϕ as defined by (22)-(27). According to (10), let $T - T_b$ be the thermal solution of (9) with $\alpha = \rho c_p$, $a = k$, $f = q$, and

- in the domain Ω_{lumen}: $b = \rho_b c_b u$ and $B = 0$;

- in the domain $\Omega_w \cup \Omega_p \cup \Omega_s$: $b = 0$ and $B = c_b \omega$.

Firstly, at the position $(r,z) \in [0; r_f[\times] - L; L[$ and the time $t > 0$, we split into

(i) $f(t) = \mu_a \frac{S(r_f,0,0)}{D\mu_t^2 - \mu_a} \exp[-\mu_{eff} vt]$ and $\iota = -\mu_{eff}$;

(ii) $f(t) = -\mu_a \frac{S(r_f,0,0)}{D\mu_t^2 - \mu_a} \exp[-\mu_t vt]$ and $\iota = -\mu_t$.

Analogously in the determination of ϕ_v we use $v_3(t) = \exp[\zeta t]/(\rho_b c_b)$ solving (14)-(15) with the factors of the $t-$argument

(i) $\zeta_1 = k\mu_{eff}^2/(\rho_b c_b) + u\mu_{eff}$.

(ii) $\zeta_2 = k\mu_t^2/(\rho_b c_b) + u\mu_t$.

Secondly, for $r_f < r < r_i$, we use $v_4(t) = \exp[\zeta_3 t]/(\rho_b c_b)$ from subsection particular solution with $\zeta_3 = k\mu_{eff}^2/(\rho_b c_b) + u\mu_t$ by taking β_b that is given in (27) into account. Next, we similarly argue for the domain $\Omega_w \cup \Omega_p \cup \Omega_s$, concluding

if $0 \le r \le r_f$:

$$T(r,z,t) = T_b + \mu_a B_0 \exp[-\mu_{eff} z] \frac{\exp[\zeta_1 t] - \exp[-\mu_{eff} vt]}{k\mu_{eff}^2 + \rho_b c_b \mu_{eff}(u+v)}$$
$$- \frac{\mu_a S(r_f,0,0)}{D\mu_t^2 - \mu_a} \exp[-\mu_t z] \frac{\exp[\zeta_2 t] - \exp[-\mu_t vt]}{k\mu_t^2 + \rho_b c_b \mu_t(u+v)}; \qquad (28)$$

if $r_f < r \le r_i$:

$$T(r,z,t) = T_b + T_1(r,z,t) + \mu_a B_0 \exp[-\mu_{eff} z] \frac{\exp[\zeta_1 t] - \exp[-\mu_{eff} vt]}{k\mu_{eff}^2 + \rho_b c_b \mu_{eff}(u+v)}$$
$$+ \left(B_1 J_0(\beta_b r) + B_2 Y_0(\beta_b r) \right) \exp[-\mu_t z] \frac{\exp[\zeta_3 t] - \exp[-\mu_t vt]}{k\mu_{eff}^2 + \rho_b c_b \mu_t(u+v)}; \qquad (29)$$

otherwise:

$$T(r,z,t) = T_o + T_1(r,z,t)$$
$$+ (B_3 W_3(\varkappa_{\lambda,j} r) + B_4 W_4(\varkappa_{\lambda,j} r)) \exp[-\mu_{eff} z] \frac{\exp\left[\zeta_4 t\right] - \exp[-\mu_{eff} vt]}{k(\mu_{eff}^{(j)})^2 - c_b \omega}$$
$$+ (B_5 J_0(\beta_j r) + B_6 Y_0(\beta_j r)) \exp[-\mu_t z] \frac{\exp\left[\zeta_4 t\right] - \exp[-\mu_t vt]}{k(\mu_{eff}^{(j)})^2 - c_b \omega}, \qquad (30)$$

where $\zeta_4 = (k(\mu_{eff}^{(j)})^2 - \rho_b c_b w)/(\rho c_p)$. Here, T_1 is the combination of radial dependent Bessel functions and longitudinal and temporal dependent exponential functions such that (11)-(13) as well as the interface continuity conditions are verified.

As the lumen Ω_{lumen} is constituted by the blood, two different situations exist:

Case 1. The blood flow is obstructed ($u = 0$), for instance the vein is completely clamped or the SSV in the presence of the inserted catheter.

Case 2. The blood flows at $u = 70\,\text{mm}\,\text{s}^{-1}$, as such it happens in the GSV. The diameter of the GSV varies from 11 mm to 12 mm at SFJ until 7.5 mm to 8 mm at the proximal thigh (at the knee level) (**Deganei & Demirkilie**, 2010)

In the case 1, T_1 is given by (20) with $Z(z) = \cosh[\eta(L - z)]$ and

$$\rho_j c_{p,j} \zeta = -k_j(\beta_{1,j}^2 + \eta^2) - c_{p,j}\omega_j \qquad j = \text{wall, pad, skin.}$$

In the case 2, the solution T_1 depends on the general form (21) of Z, and (20) takes the dependence on the vein size into account. Known values exist for diameters ranging between 3 and 10 mm, or greater than 10 mm, according to the small saphenous vein (SSV), anterior accessory vein, and great saphenous vein, namely, diameters of 7.5 mm (**Goode** *et al.*, 2010), $r_i = 3.75$ mm and $\varepsilon = 0.75$ mm, and of 1.2 cm (**Goldman**, **Mauricio**, & **Rao**, 2004), $r_i = 6$ mm and $\varepsilon = 1.2$ mm. The proposed solution may address the quantitative questions in the context of the thermal ablation treatment under study. For elucidating the effect of vein diameter, further study will be the aim of future work.

Finally, we may use the formula (28)-(30) to read the temporal course of damage events from the spatial domain. However, a first analysis should be done. Considering in (7) that $T \geq T_{\min}$, we find the following upper bound

$$t_{\text{crit}} \leq \frac{1}{A} \exp\left[\frac{E_a}{RT_{\min}}\right].$$

Next, if we use the thermal parameters from Table 3, the above upper bound of the critical time t_{crit} can be calculated (cf. Table 3) in function of different the minimum surface temperatures.

Table 3. Upper bounds of t_{crit} in seconds.

°C	blood	vein wall	perivenous tissue	skin
50	3.4e+05	5.8e+05	5.8e+05	1.1e+03
60	2.3e+03	4.7e+03	4.7e+03	9.5e-01
70	2.1e+01	5.1e+01	5.1e+01	1.3e-03
80	2.4e-01	7.2e-01	7.2e-01	2.5e-06
90	3.6e-03	1.3e-02	1.3e-02	6.9e-09
100	6.8e-05	2.8e-04	2.8e-04	2.6e-11

Then, the operating time of 10 s is a safe value for the thermal thresholds for tissue damage at the vein wall, perivenous tissue or skin, the so-called damage temperature ($T_{\min} = 50\,°C$). This value is consensual among clinicians and researchers in the ablation treatments, (**Consiglieri**, dos **Santos**, & **Haemmerich**, 2003) and the references therein. We conclude that the interpretation of the vein-tissue system damage substantially disagrees with the critical temperature of 50 °C being the temperature that temperatures above it result in necrosis.

The present result shows that the blood coagulates before the dehydration/necrosis of the wall tissue. Moreover, for the blood threshold $T_{\min} = 100\,°C$, the operating time clearly surpasses the upper bound, which is consistent with that a thin layer of carbonized blood is found to cover the fibre tip. Although according to (**Van Ruijven** *et al.*, 2014), the black layer occurs at temperatures around 300 °C. This black layer absorbs an average of 45% of the emitted light power, resulting in a decrease of the tip temperatures.

Indeed, much work remains to be done. The damage of the vein reduces to the vaporisation and occlusion in both above situations, namely cases 1 and 2. The failure and complication rates depend on vein size (**Bi** *et al.*, 2023; **Chaar** *et al.*, 2011). The influence of the pulsatile blood flow in the heat transfer is a real physiological issue in the vessels system (**Zhang** & **Xie**, 2018). Also, the perivenous tumescence injection (tumescence anesthesia) is carried on to protect the perivenous tissue from thermal damage and reduce the lumen of the truncal vein by compression and spasm (**Schmedt** *et al.*, 2010).

Conclusions

The derived solutions, namely ϕ and T, might be a tool to generate quantitative and/or qualitative results. Besides, the configurations of the physical problem solved are questioned. Our main conclusion is that the parabolic equation for the light transport leads to the application of the pulsed laser of the order of picoseconds only, while the elliptic equation leads to the physical solution for a continuous laser light.

Acknowledgment

Conflict of interests

The author declares that there is no conflict of interest.

References

Almeida, J., Mackay, E., Javier, J., Mauriello, J., Raines, J. (2009) Saphenous laser ablation at 1470 nm targets the vein wall, not blood. *Vascular and Endovascular Surgery*, *43*(5), 467–472. https://doi.org/10.1177/1538574409335916

Anchala, P., Wickman, C., Chen, R., Faundeen, T., Pearce, W., Narducy, L., Resnick, S. (2010) Endovenous laser ablation as a treatment for postsurgical recurrent saphenous insufficiency. *Cardiovascular and Interventional Radiology*, *33*(5), 983–988. https://doi.org/10.1007/s00270-009-9784-3

Ash, J. L., Moore, C. J. (2010) Laser treatment of varicose veins: Order out of chaos. *Seminars in Vascular Surgery*, *23*(2), 101–106. https://doi.org/10.1053/j.semvascsurg.2010.01.005

Bi, S., Liu, H., Nan, Q., Mai, X. (2023) Study on the effect of micro-vessels on ablation effect in laser interstitial brain tissue thermal therapy based on PID temperature control. *Applied Sciences*, *13*(6), 3751. https://doi.org/10.3390/app13063751

Bianchi, L., Cavarzan, F., Ciampitti, L., Cremonesi, M., Grilli, F., Saccomandi, P. (2022) Thermophysical and mechanical properties of biological tissues as a function of temperature: A systematic literature review. *International Journal of Hyperthermia*, *39*(1), 297–340. https://doi.org/10.1080/02656736.2022.2028908

Caggiati, A., Franceschini, M. (2010) Stroke following endovenous laser treatment of varicose veins. *Journal of Vascular Surgery*, *51*(1), 218–220. https://doi.org/10.1016/j.jvs.2009.07.092

Carradice, D., Mekako, A. I., Mazari, F. A. K., Samuel, N., Hatfield, J., Chetter, I. C. (2011) Clinical and technical outcomes from a randomized clinical trial of endovenous laser ablation compared with conventional surgery for great saphenous varicose veins. *British Journal of Surgery*, *98*(8), 1117–1123. https://doi.org/10.1002/bjs.7615

Chaar, C. I. O., Hirsch, S. A., Cwenar, M. T., Rhee, R. Y., Chaer, R. A., Hamad, G. A., Dillavou, E. D. (2011) Expanding the role of endovenous laser therapy: Results in large diameter saphenous, small saphenous, and anterior accessory veins. *Annals of Vascular Surgery*, *25*(5), 656–661. https://doi.org/10.1016/j.avsg.2011.02.031

Chebotarev, A. Y., Pak, N. M., Kovtanyuk, A. E. (2023) Analysis and numerical simulation of the initial-boundary value problem for quasilinear equations of complex

heat transfer. *Journal of Applied and Industrial Mathematics*, *17*, 698–709. https://doi.org/10.1134/S1990478923040026

Consiglieri, L. (2016) Analytical solutions in the modeling of the local RF ablation. *Journal of Mechanics in Medicine and Biology*, *16*(05), 1650071. https://doi.org/10.1142/S0219519416500718

Consiglieri, L. (2012) Continuum models for the cooling effect of blood flow on thermal ablation techniques. *International Journal of Thermophysics*, *33*(5), 864–884. https://doi.org/10.1007/s10765-012-1194-0

Consiglieri, L. (2013) An analytical solution for a bio-heat transfer problem. *International Journal of Bio-Science and Bio-Technology*, *5*(5), 267–278. https://doi.org/10.14257/ijbsbt.2013.5.5.26

Consiglieri, L., dos Santos, I., Haemmerich, D. (2003) Theoretical analysis of the heat convection coefficient in large vessels and the significance for thermal ablative therapies. *Physics in Medicine and Biology*, *48*(24), 4125–4134. https://doi.org/10.1088/0031-9155/48/24/010

Doganci, S., Demirkilic, U. (2010) Comparison of 980 nm laser and bare-tip fibre with 1470 nm laser and radial fibre in the treatment of great saphenous vein varicosities: A prospective randomised clinical trial. *European Journal of Vascular and Endovascular Surgery*, *40*(2), 254–259. https://doi.org/10.1016/j.ejvs.2010.04.006

Etlik, Ö., Korkmaz, A. A., Üçkurt, Y., Indelen, S., Gündoğdu, R., Öztürk, A., al-Salehi, S. K., Aung, S. M. (2013) Endovenous laser ablation for saphenous vein insufficiency: Long-term results. *Turkish Journal of Medical Sciences*, *43*(3), 470–473. https://doi.org/10.3906/sag-1206-68

Firouznia, K., Ghanaati, H., Hedayati, M., Shakiba, M., Jalali, A. H., Mirsharifi, R., Dargahi, A. (2013) Endovenous laser treatment (EVLT) for the saphenous reflux and varicose veins: A follow-up study. *Journal of Medical Imaging and Radiation Oncology*, *57*(1), 15–20. https://doi.org/10.1111/j.1754-9485.2012.02457.x

Gale, S. S., Lee, J. N., Walsh, M. E., Wojnarowski, D. L., Comerota, A. J. (2010) A randomized, controlled trial of endovenous thermal ablation using the 810-nm wavelength laser and the ClosurePLUS radiofrequency ablation methods for superficial venous insufficiency of the great saphenous vein. *Journal of Vascular Surgery*, *52*(3), 645–650. https://doi.org/10.1016/j.jvs.2010.04.030

Goldman, M., Mauricio, M., Rao, J. (2004) Intravascular 1320-nm laser closure of the Great Saphenous Vein: A 6- to 12-month follow-up study. *Dermatologic Surgery*, *30*(11), 1380–1385. https://www.ncbi.nlm.nih.gov/pubmed/15522018

González-Suárez, A., Trujillo, M., Burdío, F., Andaluz, A., Berjano, E. (2014) Could the heat sink effect of blood flow inside large vessels protect the vessel wall from thermal damage during RF-assisted surgical resection? *Medical Physics*, *41*(8), 083301. https://doi.org/10.1118/1.4890103

Goode, S., Chowdhury, A., Crockett, M., Beech, A., Simpson, R., Richards, T., Braithwaite, B. (2010) Laser and radiofrequency ablation study (LARA study): A randomised study comparing Radiofrequency Ablation and Endovenous Laser Ablation (810nm). *European Journal of Vascular and Endovascular Surgery*, *40*(2), 246–253. https://doi.org/10.1016/j.ejvs.2010.02.026

Horng, T.-L., Lin, W.-L., Liauh, C.-T., Shih, T.-C. (2007) Effects of pulsatile blood flow in large vessels on thermal dose distribution during thermal therapy. *Medical Physics*, *34*(4), 1312–1320. https://doi.org/10.1118/1.2712415

Katta, N., Santos, D., McElroy, A. B., Estrada, A. D., Das, G., Mohsin, M., Donovan, M., Milner, T. E. (2022) Laser coagulation and hemostasis of large diameter blood vessels: Effect of shear stress and flow velocity. *Scientific Reports*, *12*, 8375. https://doi.org/10.1038/s41598-022-12128-1

Kotte, A. N. T. J., van Leeuwen, G. M. J., Lagendijk, J. J. W. (1999) Modelling the thermal impact of a discrete vessel tree. *Physics in Medicine & Biology*, *44*(1), 57–74. https://doi.org/10.1088/0031-9155/44/1/006

Marqa, M., Mordon, S., Hernandez-Osma, E., Trelles, M., Betrouni, N. (2013) Numerical simulation of endovenous laser treatment of the incompetent great saphenous vein with external air cooling. *Lasers in Medical Science*, *28*(3), 833–844. https://doi.org/10.1007/s10103-012-1141-0

Memetoglu, M. E., Erbasan, O., Özel, D. (2012) Follow-up results of laser saphenous ablation. *Dicle Tip Dergisi*, *39*(3), 331–335. https://doi.org/10.5798/diclemedj.0921.2012.03.0153

Min, R. J., Khilnani, N. M., Zimmet, S. E. (2003) Endovenous laser treatment of saphenous vein reflux: Long-term results. *Journal of Vascular and Interventional Radiology*, *14*(8), 991–996. https://doi.org/10.1097/01.RVI.0000082864.05622.E4

Mordon, S., Wassmer, B., Zemmouri, J. (2006) Mathematical modeling of endovenous laser treatment (ELT). *BioMedical Engineering OnLine*, *5*, 26. https://doi.org/10.1186/1475-925X-5-26

Oh, C. K., Jung, D.-S., Jang, H. S., Kwon, K. S. (2003) Endovenous laser surgery of the incompetent Greater Saphenous Vein with a 980-nm diode laser. *Dermatologic Surgery*, *29*(11), 1135–1140. https://www.ncbi.nlm.nih.gov/pubmed/14641341

Olver, F. (1972) Bessel functions of integer order. In M. **Abramonitz** I. **Stegun** (Eds.), *Handbook of mathematical functions with formulas, graphs, and mathematical tables* (pp. 355–389).

Özisik, M. (2012) Appendix IV: Bessel Functions. In *Heat conduction* (pp. 691–706). John Wiley & Sons, Ltd. https://doi.org/10.1002/9781118411285.app4

Özkan, U., Saritürk, C. (2012) Early clinical improvement in chronic venous insufficiency symptoms after laser ablation of saphenous veins. *Diagnostic and Interventional Radiology*, *18*(6), 594–598. https://doi.org/10.4261/1305-3825.DIR.5917-12.1

Palombi, L., Morelli, M., Bruzzese, D., Martinelli, F., Quarto, G., Bianchi, P. G. (2024) Endovenous laser ablation (EVLA) for vein insufficiency: two-year results of a multicenter experience with 1940-nm laser diode and a novel optical fiber. *Lasers in Medical Science*, *39*, 61. https://doi.org/10.1007/s10103-024-04000-7

Poluektova, A., Malskat, W., Gemert, M. V., Vuylsteke, M., Bruijninckx, C., Neumann, H., van der Geld, C. (2014) Some controversies in endovenous laser ablation of varicose veins addressed by optical-thermal mathematical modeling. *Lasers in Medical Science*, *29*, 441–452. https://doi.org/10.1007/s10103-013-1450-y

Prahl, S. A. (1995) The diffusion approximation in three dimensions. In A. J. **Welch** M. J. C. **Van Gemert** (Eds.), *Optical-thermal response of laser-irradiated tissue* (pp. 207–231). Springer US.

Prince, E., Soares, G., Silva, M., Taner, A., Ahn, S., Dubel, G., Jay, B. (2011) Impact of laser fiber design on outcome of endovenous ablation of lower-extremity varicose veins: Results from a single practice. *Cardiovascular and Interventional Radiology*, *34*(3), 536–541. https://doi.org/10.1007/s00270-010-9922-y

Proebstle, T., Krummenauer, F., Gul, D., Knp, J. (2004) Nonocclusion and early reopening of the great saphenous vein after endovenous laser treatment is fluence dependent. *Dermatologic Surgery*, *30*, 174–178. https://doi.org/10.1067/mva.2002.121132

Puggioni, A., Kalra, M., Carmo, M., Mozes, G., Gloviczki, P. (2005) Endovenous laser therapy and radiofrequency ablation of the great saphenous vein: Analysis of early efficacy and complications. *Journal of Vascular Surgery*, *42*(3), 488–493. https://doi.org/10.1016/j.jvs.2005.05.014

Rasmussen, L. H., Lawaetz, M., Bjoern, L., Vennits, B., Blemings, A., Eklof, B. (2011) Randomized clinical trial comparing endovenous laser ablation, radiofrequency ablation, foam sclerotherapy and surgical stripping for great saphenous varicose

veins. *British Journal of Surgery*, *98*(8), 1079–1087. https://doi.org/10.1002/bjs.7555

Rathod, J., Taori, K., Joshi, M., Mundhada, R., Rewatkar, A., Dhomane, S., Gour, P. (2010) Outcomes using a 1470-nm laser for symptomatic varicose veins. *Journal of Vascular and Interventional Radiology*, *21*(12), 1835–1840. https://doi.org/10.1016/j.jvir.2010.09.009

Roggan, A., Friebel, M., Doerschel, K., Hahn, A., Mueller, G. J. (1999) Optical properties of circulating human blood in the wavelength range 400-2500 nm. *Journal of Biomedical Optics*, *4*(1), 36–46. https://doi.org/10.1117/1.429919

Schmedt, C.-G., Blagova, R., Karimi-Poor, N., Burgmeier, C., Steckmeier, S., Beck, T., Hecht, V., Meier, R., Sadeghi-Azandaryani, M., Steckmeier, B., Sroka, R. (2010) Update of endovenous laser therapy and the latest application studies. *Medical Laser Application*, *25*(1), 34–43. https://doi.org/10.1016/j.mla.2009.11.004

Schwarz, T., von Hodenberg, E., Furtwängler, C., Rastan, A., Zeller, T., Neumann, F.-J. (2010) Endovenous laser ablation of varicose veins with the 1470-nm diode laser. *Journal of Vascular Surgery*, *51*(6), 1474–1478. https://doi.org/10.1016/j.jvs.2010.01.027

Sharif, M. A., Soong, C. V., Lau, L. L., Corvan, R., Lee, B., Hannon, R. J. (2006) Endovenous laser treatment for long saphenous vein incompetence. *British Journal of Surgery*, *93*(7), 831–835. https://doi.org/10.1002/bjs.5351

Star, W. M. (1995) Diffusion theory of light transport. In A. J. **Welch** M. J. van **Gemert** (Eds.), *Optical-thermal response of laser-irradiated tissue* (pp. 131–206). Springer US.

Theivacumar, N., Gough, M. (2011) Endovenous Laser Ablation (EVLA) to Treat Recurrent Varicose Veins. *European Journal of Vascular and Endovascular Surgery*, *41*(5), 691–696. https://doi.org/10.1016/j.ejvs.2011.01.018

Tseng, Y.-H., Chen, C.-W., Wong, M.-Y., Yang, T.-Y., Lin, Y.-H., Lin, B.-S., Huang, Y.-K. (2022) Blood flow analysis of the great saphenous vein in the su-pine position in clinical manifestations of varicose veins of different severities: Application of phase-contrast magnetic resonance imaging data. *Diagnostics*, *12*(1). https://doi.org/10.3390/diagnostics12010118

Van Ruijven, P., Poluektova, A., Van Gemert, M., Neumann, H., Nijsten, T., Van der Geld, C. (2014) Optical-thermal mathematical model for Endovenous Laser Ablation of varicose veins. *Lasers in Medical Science*, *29*, 431–439. https://doi.org/10.1007/s10103-013-1451-x

Vuylsteke, M., Martinelli, T., Van Dorpe, J., Roelens, J., Mordon, S., Fourneau, I. (2011) Endovenous Laser Ablation: The role of intraluminal blood. *European Journal of Vascular and Endovascular Surgery*, *42*(1), 120–126. https://doi.org/10.1016/j.ejvs.2011.03.017

Zhang, Y., Xie, H. (2018) The effect of a bifurcation structure on the heat transfer and temperature distribution of pulsatile blood flow. *International Journal of Heat and Mass Transfer*, *118*, 663–670. https://doi.org/10.1016/j.ijheatmasstransfer.2017.11.055